Remote Sensing of Environment 182 (2016) 49–59

Contents lists available at ScienceDirect

Remote Sensing of Environment

journal homepage: www.elsevier.com/locate/rse

A multi-sensor approach towards a global vegetation corrected SRTM DEM product

F.E. O'Loughlin [a,*], R.C.D. Paiva [b], M. Durand [c], D.E. Alsdorf [c], P.D. Bates [a]

[a] School of Geographical Sciences, University of Bristol, United Kingdom
[b] Institute of Hydraulic Research, Federal University of Rio Grande do Sul, Brazil
[c] School of Earth Science and Byrd Polar and Climate Research Center, Ohio State University, United States

ARTICLE INFO

Article history:
Received 21 May 2015
Received in revised form 13 April 2016
Accepted 27 April 2016
Available online 18 May 2016

Keywords:
SRTM
Vegetation correction
Digital Elevation Model
DEM
ICESat
Bare-Earth

ABSTRACT

We develop the first global 'Bare-Earth' Digital Elevation Model (DEM) based on the Shuttle Radar Topography Mission (SRTM) for all landmasses between 60N and 54S. Our new 'Bare-Earth' SRTM DEM combines multiple remote sensing datasets, including point-ground elevations from NASA's laser altimeter ICESat, a database of percentage of tree cover from the MODIS satellite as a proxy for penetration depth of SRTM and a global vegetation height map in order to remove the vegetation artefacts present in the original SRTM DEM. We test multiple methods of removing vegetation artefacts and investigate the use of regionalization. Our final 'Bare-Earth' SRTM product shows global improvements greater than 10 m in the bias over the original SRTM DEM in vegetated areas compared with ground elevations determined from ICESat data with a significant reduction in the root mean square error from over 14 m to 6 m globally. Therefore, our DEM will be valuable for any global applications, such as large scale flood modelling requiring a 'Bare-Earth' DEM.

1. Introduction

Digital Elevation Models (DEMs) are used for a wide range of applications, including hydrology and water resources, geology and geomorphology, civil engineering projects, vegetation survey, glaciology, volcanology and modelling natural hazards such as flooding, landslides and coastal inundation (Bamber, 1994; Moore, Grayson, and Ladson, 1991). The accuracy of such DEMs is a key point for these applications. For example, in river hydrodynamic modelling, the DEM is one of the most important inputs as it controls the accuracy of the model outputs (Sanders, 2007), in particular flood extents and depths. With climate change, development pressures, and land-use changes generally leading to changes in flood frequencies globally (Hirabayashi et al., 2013; Milly, Wetherald, Dunne, and Delworth, 2002), accurate outputs from hydrodynamic models will become increasingly necessary to understand the risks associated with these changes and their impact on global wetlands and associated issues related to biogeochemical cycles and biodiversity.

In many developed nations accurate DEMs derived from expensive LiDAR surveys are now available, with the first LiDAR surveys flown in the 1980s (Krabill, Collins, Link, Swift, and Butler, 1984). However, these only cover a small percentage of the earth's landmass. For global or near global coverage, space based DEMs must be used. To date, the most popular near-global DEM was obtained from Shuttle Radar Topography Mission — SRTM (Farr et al., 2007). The SRTM DEM has been used by numerous scientists for a variety of science studies. However, all these studies have encountered the same issue: how to correct the vegetation bias in the SRTM DEM. Schumann, Bates, Neal, and Andreadis (2014) noted the importance of an accurate 'Bare-Earth' DEM for flood-modelling and related industries. Baugh, Bates, Schumann, and Trigg (2013) noted that correcting the vegetation error in the SRTM DEM for a region of the Amazon Basin increased the accuracy of modelled inundation extents from 25% to 94%.

Carabajal and Harding (2005) validated the SRTM DEM using ICESat, a satellite laser altimeter, and discovered that the errors in SRTM increased with increasing tree cover. This was because the C-band radar used by SRTM could not fully penetrate the vegetation canopy to the ground. This finding was also supported by another study that utilized satellite radar altimeters to validate the SRTM DEM (Berry, Garlick, and Smith, 2007). While these errors can clearly be attributed to vegetation, their correction requires knowledge about canopy heights and radar penetration depths. The first widely used global vegetation height map was only published in 2010 (Lefsky, 2010), followed by a more accurate vegetation map the following year (Simard, Pinto, Fisher, and Baccini, 2011). Prior to this, the correction of vegetation biases in SRTM could only be undertaken on small areas using either in-situ measurements or national datasets (Gallant, Read, and Dowling, 2012; Wilson et al., 2007). In hydrologic and hydrodynamic modelling, vegetation errors in the SRTM have generally been ignored except in

* Corresponding author.
E-mail address: fiachra.oloughlin@bristol.ac.uk (F.E. O'Loughlin).

http://dx.doi.org/10.1016/j.rse.2016.04.018

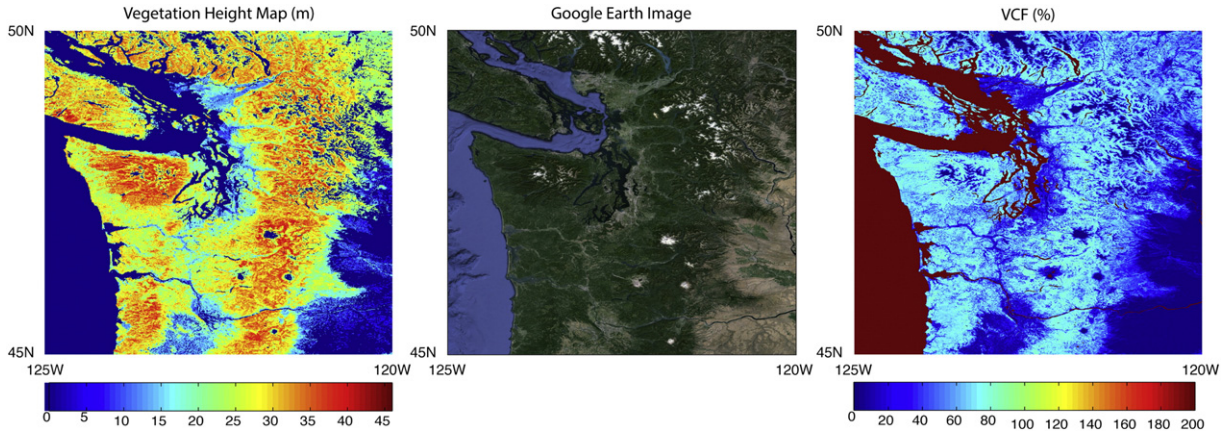

Fig. 1. Comparison of Vegetation Height Map, Google Earth Image and VCF product. Examples of the Vegetation Height Map and VCF datasets are shown for a smaller region in Fig. 9.

heavily-vegetated areas, such as the Amazon (De Ruyver, 2004; Pinel et al., 2015). However, here the SRTM bias can cause large errors in model results such as under predicted flood extent and too rapid flood wave propagation (Jarihani, Callow, McVicar, Van Niel, and Larsen, 2015; Paiva et al., 2013). Despite the importance of artefact removal methods to correct vegetation errors in SRTM data to date have been rather simple and have only applied static corrections, i.e. they removed a spatially uniform fixed percentage of vegetation height from the DEM (e.g. Baugh et al., 2013; Paiva, Collischonn, and Tucci, 2011). For example, Baugh et al. (2013) found that subtracting 50% of the vegetation height produced the best results in their hydrodynamic model but highlighted that this fraction may be different in other regions with other vegetation densities.

In this study we therefore introduce a first near global 'Bare-Earth' SRTM DEM product using a dynamic correction that varies with vegetation height and density, and which can be regionalized according to climatic zones or vegetation types. Our 'Bare-Earth' SRTM DEM deals only with vegetation biases and does not remove biases due to built structures.

2. Data and methodology

We use the SRTM DEM as our base data product. We then use global maps of vegetation height (Simard et al., 2011) and a canopy density proxy from MODIS data, coupled with satellite altimetry (ICESat GLAS) to develop and validate an empirical model for global DEM vegetation correction. Different correction models and parameter regionalizations are tested and to determine an optimal method, examples showing the impact of the vegetation correction on the SRTM DEM are provided. All datasets used were horizontally referenced to WGS84.

2.1. SRTM DEM

The Shuttle Radar Topography Mission (SRTM) (Farr et al., 2007) was an international project sponsored by the National Geospatial-Intelligence Agency (NGA) and NASA and was flown in February 2000. During its 11 day mission 12.3 Tbyte of terrain data were collected covering land areas between 56S and 60N. Two InSAR instruments were used: a C-band radar provided by the Jet Propulsion Laboratory (JPL) and an X-band radar provided by the German and Italian space agencies.

Kinematic GPS transects, corner reflector arrays, ground control points (GCPs) from NGA and JPL, and optical imagery DEMs were used in system calibration and accuracy assessment (Farr and Kobrick, 2000). SRTM's vertical and horizontal linear errors at 90% confidence (LE90) were smaller than the mission specifications of 20 m and 16 m respectively (Rabus, Eineder, Roth, and Bamler, 2003). When compared with GCPs, Rodríguez, Morris, and Belz (2006) discovered that vertical errors (LE90) in SRTM were approximately 8.2 m globally, while Berry et al. (2007) found the vertical mean error globally between SRTM and ground points determined from satellite radar altimetry data to be 3.6 ± 16.16 m.

In this study, we used the 3 arc-second C-band void-filled version 4 SRTM DEM product (Jarvis, Reuter, Nelson, and Guevara, 2008) obtained from the Consortium for Spatial Information (CGIAR CSI) available at srtm.csi.cgiar.org. This product is referenced vertically to the Earth Gravitational Model of 1996 (EGM96). EGM96 has the same reference ellipsoid as WGS84, but it has a higher spatial resolution and more accurate geoid. While many different versions of the SRTM DEM exist, all of them have the same vegetation errors and the method described below is generic.

2.2. ICESat

The ICESat Geoscience Laser Altimeter System (GLAS) was the first satellite based Earth orbiting laser altimeter and was operational between 2003 and 2009. ICESat GLAS had a surface footprint of ~65 m and made observations every 172 m along its track (Schutz, Zwally, Shuman, Hancock, and DiMarzio, 2005). Mission details and data products are described by Zwally et al. (2002). In this study the ICESat GLAS GLA14 Land Elevation Product, Release 34, was used. Geodetic and atmospheric corrections have already been applied to this product. Carabajal and Harding (2005) noted that the vertical error in these data is 0.01 ± 0.04 m for flat surfaces.

ICESat data were obtained from the Reverb website (available at reverb.echo.nasa.gov) and were extracted using code provided by the National Snow and Ice Data Centre (NSIDC). The extracted data were converted to the WGS84. Suitable observations were selected by use of the elevation-use flag, and the saturation index was used to remove/correct saturated observations. This was done to ensure only undistorted ground elevations were selected. The same criteria used by Hall, Schumann, Bamber, Bates, and Trigg (2012) and O'Loughlin, Neal, Yamazaki, and Bates (2016); O'Loughlin, Trigg, Schumann, and Bates (2013) was implemented: observations with a saturation index less than two were not corrected, observations with an index of two were corrected using the saturation elevation correction field, and all other observations were excluded. The selected observations were then converted to EGM96 — the same vertical datum as the SRTM DEM. However, as a number of peaks can be found in ICESat GLA14 observations and the GLA14 elevation is given as the centroid of the Gaussian fit, to ensure that the ICESat returns are as close as possible to 'ground truth' we applied the criterion that the number of peaks detected in the ICESat observations must be equal to one. We use the centroid value as this is the best estimate of the mean ground elevation over the ~70 m ICESat return for single peak waveforms. It should be noted that the returns of single peak data over vegetation are wider than multiple peak returns. While it is known that ICESat suffers from errors due to changes in

surface slope, canopy density and vegetation type (Bhang, Schwartz, and Braun, 2007), in this study we assume that the single peak ICESat observations are 'ground-truth', while in fact they may be slightly above the ground elevation due to the Gaussian fit.

2.3. Vegetation height map

In this study we use the vegetation height map, H_{VEG}, produced by Simard et al. (2011). This used the RH100 metric calculated from the ICESat GLAS GLA14 land product as the measure of canopy height for each observation. RH100 is the distance between the beginning of signal and the ground peak (Harding and Carabajal, 2005). Using a slope map produced from SRTM, (Simard et al., 2011) also estimated and corrected the bias in canopy heights introduced by slopes. Simard et al. (2011) used the Random Forest regression tree method to extrapolate the RH100 values based on seven variables to create their vegetation height map. These seven variables are global mean precipitation, precipitation seasonality, mean temperature, temperature seasonality, elevation, MODIS tree cover and protection status and were used to create the vegetation height map at a spatial resolution of 30 arc-seconds (~1 km). Simard et al. (2011) validated their near-global vegetation height map at 66 FLUXNET sites and calculated a root mean square error (RMSE) of 6.1 m using all sites and a RMSE of 4.4 m without 7 outliers. FLUXNET sites are parts of a global network of micrometeorological towers at which canopy heights were also recorded (Baldocchi et al., 2001). A comparison of the Vegetation Height Map to a Google Earth Image and canopy density is shown in Fig. 1.

2.4. Canopy density

In this study we use data from the 250 m MODIS Vegetation Continuous Field (VCF) product (DiMiceli et al., 2011) (available from landcover.org) as a proxy of canopy density and penetration depth of SRTM. The VCF contains three products available from 2000 to 2009: percentage area of tree cover, percentage area of non-tree vegetation and 'Bare-Earth'. In this study we only use the percent tree cover dataset from 2000 as this was the year the SRTM was flown. The values in this dataset range from 0 to 200, where any value over 100 is classified as water. For more details on the development of the VCF product see Hansen et al. (2003). Higher resolution vegetation maps are available (e.g. Landsat VCF (Sexton et al., 2013) or the ALOS PALSAR global forest mosaic (Shimada et al., 2014)) but as these datasets contain significant striping errors or are not available for the year 2000, their use would require sophisticated processing and for the first version of the 'Bare-Earth' SRTM DEM the 250 m MODIS VCF product is preferred.

2.5. Regionalization maps

Two different maps were used for regionalization. The first uses the five main Koppen-Geiger climatic classifications (Peel, Finlayson, and McMahon, 2007) and the second uses the 15 land cover type classifications derived from the MODIS Land Cover Type (MCD12Q1) product from 2001 to 2010 (Broxton, Zeng, Sulla-Menashe, and Troch, 2014). The Koppen-Geiger climate classification is available at 0.1° spatial resolution and the five zones are Tropical, Arid, Temperate, Cold and Polar. The spatial resolution of the MODIS-based land cover is 15 arc-seconds (~500 m).

2.6. Methodology

2.6.1. Outlier removal

For each ICESat ground elevation observation we extracted the corresponding pixel values from the SRTM DEM, the VCF, the Simard et al. (2011) vegetation height map and the climate and vegetation type classifications. Prior to this we re-sampled both the VCF and vegetation height maps from their native resolution to 3 arc-seconds. A nearest neighbour interpolation was used on the VCF dataset and for the vegetation height map we converted it to a point dataset and then used linear interpolation to create a 3 arc-second surface. We then removed all ICESat observations with a VCF value corresponding to water, leaving 213,214,740 ICESat observations that correspond to values over land.

For these remaining ICESat observations, we first removed any observations with a corresponding VCF or H_{VEG} pixel value equal to zero, as we are only interested in correcting the vegetation bias in the SRTM DEM. Then we subtracted the ICESat elevations from the corresponding SRTM elevations to find the residual error. Obvious outliers were removed by comparing the residual to a predefined range. This range was determined by combining the typical errors associated with SRTM with the height errors in the vegetation height map. Combining these errors, at LE90, results in a total error of ~11 m, as LE90 for SRTM 7.0 m (Rodríguez et al., 2006) and LE90 for the vegetation height map is approximately 7.3 m. Therefore, the range is defined as $H_{VEG} \pm 11$ m. After applying these criteria, we were left with 129,659,538

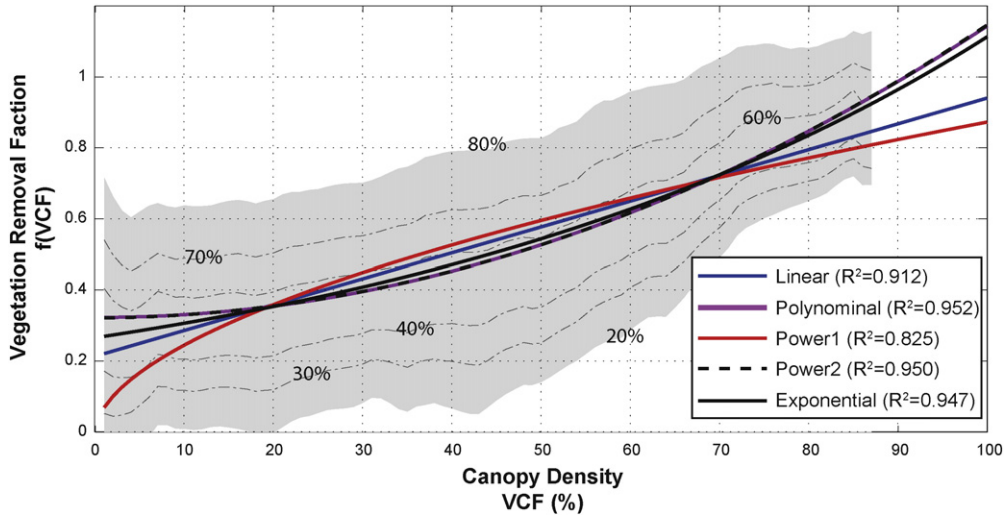

Fig. 2. Vegetation Correction Function Curves for the global fit. X-axis shows the canopy density and Y-axis shows the vegetation removal fraction. Shaded areas shows the calibration area between 20 and 80 percentiles, also shown are the 30, 40, 60 and 70 percentiles.

Table 1
Root mean square error (m) and vertical mean error (m) for the five Vegetation Correction Function Curves for the global fit shown in Fig. 1.

f(VCF)	RMSE	ME
Linear	6.17	−0.99
Polynomial	6.24	−0.84
Power 1	6.11	1.18
Power 2	7.93	2.81
Exponential	6.20	−0.87

observations to use for both calibration and validation of our vegetation correction method.

2.6.2. Vegetation removal function

The following assumptions were used in our method for correcting vegetation errors in the SRTM DEM:

- The percentage of the vegetation height (H_{VEG}) to be subtracted from the SRTM DEM is related to the canopy density (VCF).
- The Vegetation Continuous Field (VCF) is an accurate representation of the density of the canopy.

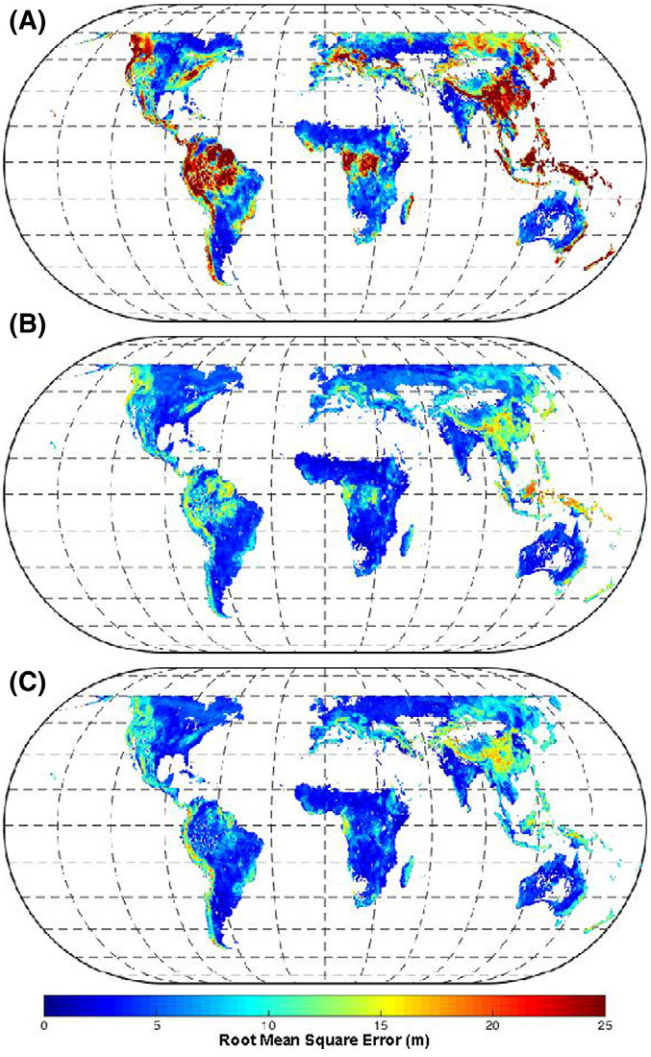

Fig. 3. Root mean square error (m) in vegetated areas for: A) SRTM; B) SRTM with static correction applied; and C) SRTM with global Power 1 correction applied. Maps display at 0.5° spatial resolution. ICESat GLA14 elevation used for validation.

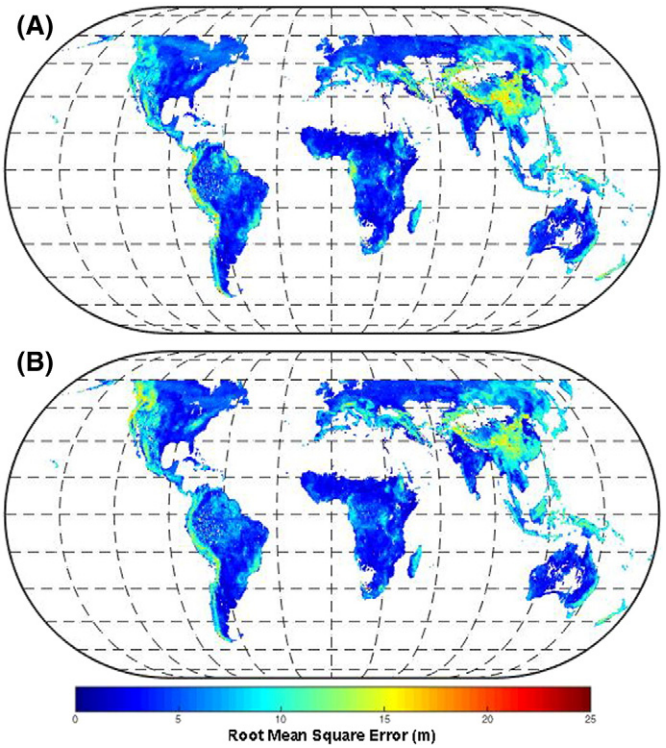

Fig. 4. Root mean square error (m) in vegetated areas for: A) SRTM with climatic Power 1 correction applied (best overall method); and B) SRTM with vegetation Power 1 correction applied. Maps display at 0.5° spatial resolution. ICESat GLA14 elevations used for validation.

- The ICESat GLA14 measurements measure the 'Bare-Earth' or ground elevations.
- The amount of vegetation to be removed, Veg_{rm}, can be represented by:

$$Veg_{rm} = f(VCF)H_{VEG} \quad (1)$$

The equation for the 'Bare-Earth' SRTM is then represented by:

$$SRTM_{Bare\text{-}Earth} = SRTM - Veg_{rm}. \quad (2)$$

By combining Eq. (1) and Eq. (2) and substituting ICESat measurements for the 'Bare-Earth' SRTM, the fraction of vegetation height to be removed can be calculated for each ICESat observation as:

$$f(VCF) = \frac{SRTM - ICESat}{H_{VEG}}. \quad (3)$$

Five different forms (Eqs. (4)–(8)) of f(VCF) were tested to estimate the percentage of H_{VEG} to be removed.

$$\text{Linear}: f(VCF) = aVCF + b \quad (4)$$

$$\text{Polynominal}: f(VCF) = aVCF^2 + bVCF + c \quad (5)$$

$$\text{Power 1}: f(VCF) = aVCF^b \quad (6)$$

$$\text{Power 2}: f(VCF) = aVCF^b + c \quad (7)$$

$$\text{Exponential}: f(VCF) = a\exp^{bVCF}. \quad (8)$$

The parameters of these functions were fitted based on ICESat samples (Eq. (3)). Because using the entire dataset would result in no

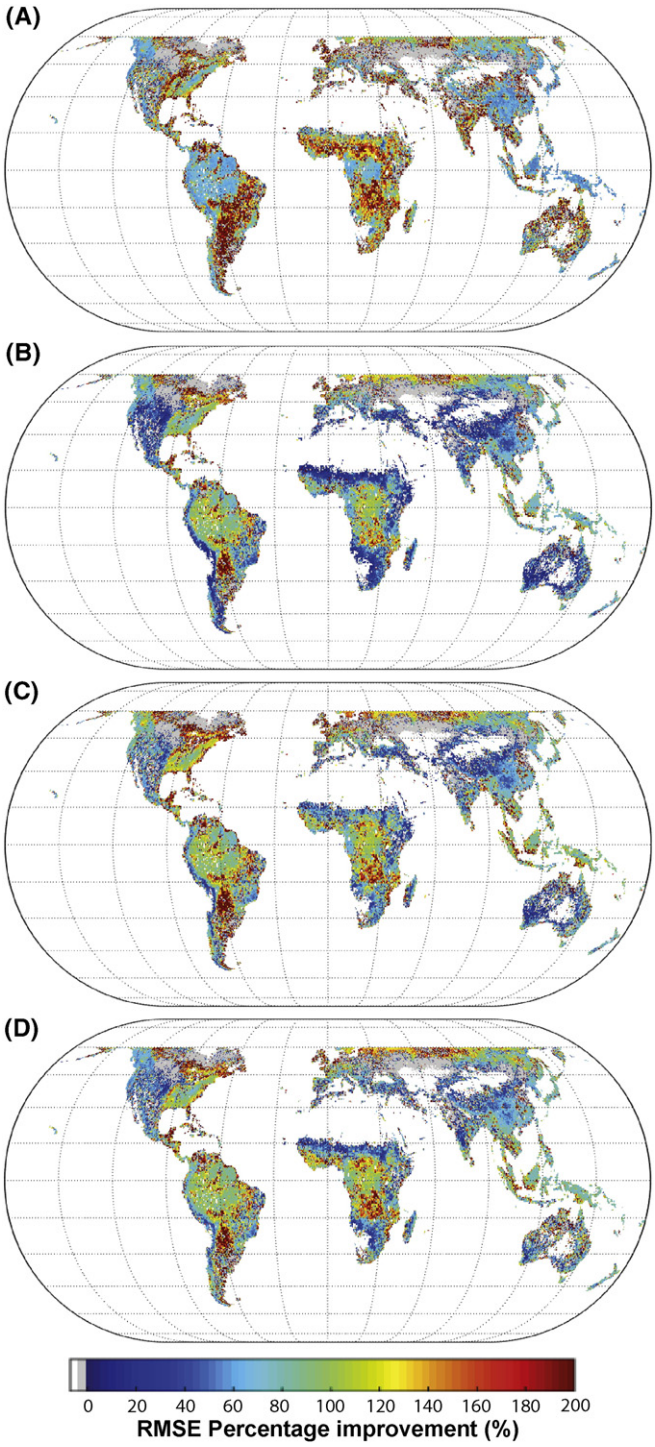

Fig. 5. Percentage improvement in root mean square error (RMSE) over the original SRTM compared with ICESat ground elevations for: (A) SRTM with static correction applied; (B) SRTM with global Power 1 correction applied; (C) SRTM with climatic Power 1 correction applied (best overall method); and (D) SRTM with vegetation Power 1 correction applied. Areas where the vegetation correction results in a deterioration of errors are shaded grey.

independent data to validate the method, we repeatedly fit the model to 1% of the total dataset, randomly sampled, to create 10,000 fits, using least squares. However, to ensure that each VCF value is given equal weight, before fitting the function we average the data by VCF value and then the function is fitted to the VCF averaged data. The final f(VCF) curve was computed by averaging results from the 10,000 fitted curves. As a single parameter set for the f(VCF) model may not be valid for the whole globe, we also tested regionalized parameters as functions of climate zones or vegetation types.

2.6.3. Global vegetation removal

The global vegetation corrected products were produced using the globally available VCF and vegetation height maps. For each SRTM tile, the fraction of H_{VEG} to be removed was calculated pixel-by-pixel using the best vegetation removal function found (see Section 3.1) and the corresponding VCF value. For the regionalized maps, the regional classification of each pixel was also taken into account. Once the fraction of H_{VEG} to be removed was determined, this was multiplied by the corresponding pixel value of H_{VEG} and this dataset was then subtracted from the original SRTM elevations.

2.6.4. Performance metrics

To determine the best performing vegetation removal function, we compare the produced 'Bare-Earth' SRTM DEMs to ICESat measurements using two different metrics: root mean square error (RMSE) and mean error (ME). These were estimated both globally and by continent.

To ensure that the performance metrics were not biased by the large amount of data corresponding to lower VCF values, we also calculated the metrics with data averaged by VCF value as well as by assigning equal weights to the observations.

3. Results and discussion

3.1. Comparison of vegetation correction functions

We plotted the five global vegetation correction functions, f(VCF), against the Vegetation Continuous Field (VCF) data (Fig. 2). It was expected that the curves would be similar to each other with the value of f(VCF) increasing with canopy density (VCF value). However, it was expected that the curves would become asymptotic for higher canopy density (VCF values) as we expected the penetration depth of SRTM would become near constant for higher canopy densities. This assumption is based on the work of Kenyi, Dubayah, Hofton, and Schardt (2009) who found C-Band SRTM penetrated on average 56% into the canopy of a forest area in the Sierra Nevada; however, they also noted that if a canopy is thick and homogeneous, a smaller penetration depth would be expected. It was also expected that the value of f(VCF) would tend to zero for lower canopy density.

While Fig. 2 shows that all f(VCF) models are similar for VCF values between 20 and 80, only the Power 1 model followed the expected curve. However, models with f(VCF) values greater than one cannot be discarded, as the raw vegetation height map is an average value over 1 km^2 (which we resample to 3 arc-seconds) and variations in height are possible, resulting in f(VCF) values greater than one. At lower canopy densities, again only the Power 1 model followed the expected pattern. Table 1 shows the root mean square error (m) and the vertical mean error (m) for the five f(VCF) models fitted globally when compared with ICESat GLA14 elevations. Also listed in Fig. 2 are the corresponding R^2 values obtained for each of the five models when compared to data averaged by VCF values. It is clear that the Power 1 model results in the lowest RMSE while having a similar vertical ME compared with the four other f(VCF) models. While no models could be discarded based on higher canopy density values, all models, with the exception of the Power 1 model, introduce artefacts at low canopy densities. All the models tested could have been forced to follow our expected curve by setting their intercept equal to zero and one, i.e. when VCF = 0, f(VCF) = 0 and when VCF = 100, f(VCF) = 1; however, this would skew the results to fit our initial assumptions and therefore no longer allow the data to be independent. As a consequence, the Power 1 model was determined to be the best method that we tested to correct the vegetation error in the SRTM DEM.

Table 2
Root mean square error (m) of RAW and corrected SRTM using different vegetation correction methods compared with ICESat GLA14 elevations in vegetated areas. Both averaged by VCF (1st number) and equal weight (2nd number) calculations are shown.

Region	Vegetation correction method				
	Raw	Static	Global	Climate	Vegetation
Europe	13.359/9.689	7.058/6.125	5.853/5.125	5.530/4.989	5.840/4.975
Africa	12.619/6.083	6.039/3.538	4.826/4.000	4.753/3.676	4.673/3.679
Asia	16.889/11.971	9.151/7.250	7.802/7.198	7.526/6.894	7.473/6.682
Southern Asia	18.656/12.865	9.742/7.032	7.764/5.966	7.020/5.424	7.114/5.390
Australia & New Zealand	16.514/7.326	8.774/4.564	6.915/4.655	6.686/4.427	6.634/4.259
Pacific Islands	20.588/21.018	10.976/11.207	10.361/10.517	9.263/9.386	9.201/9.267
North America	12.012/7.978	7.182/5.492	6.027/5.311	6.028/5.354	6.562/5.160
South America	12.190/8.126	6.412/4.756	5.200/4.554	5.136/4.389	4.978/4.191
Global	14.116/8.667	7.576/5.292	6.108/5.185	5.939/4.980	6.035/4.854

3.2. Comparison of static, global and regional based vegetation correction

To determine the best vegetation correction method to apply to the SRTM DEM, we compared a static correction, where a spatial uniform percentage of H_{VEG} was removed from the SRTM DEM, and the proposed method, where a spatial varying percentage of H_{VEG} is removed from the SRTM DEM. The static correction method removes 50% of H_{VEG} from the SRTM DEM, as suggested by Baugh et al. (2013), while the proposed method calculated f(VCF) used the Power 1 correction function (Eq. (6)) fitted both globally and by region using classification maps of climate zone and vegetation type, with unique f(VCF) functions calculated for each distinct region, using the same methodology as for the global fit.

For each method we calculated the RMSE and ME by comparing the DEMs to ICESat GLA14 elevations, and then compared the results both visually and statistically. Visual comparison was performed on 0.5 degree resolution plots (Figs. 3, 4 and 5), where observations within each 0.5 degree square were averaged. The statistical comparison was undertaken both globally and by continent (Tables 2 and 3) at locations where ICESat ground elevations exist.

From Figs. 3 and 5, it is clear that any form of vegetation removal improves the SRTM DEM in most regions of the globe. Areas where the methods tested cause deterioration in errors are shaded grey in Fig. 5. Despite being the simplest method, the static correction (Fig. 3(B)) removes much of the vegetation error in the SRTM DEM. Globally the static method reduces the vertical bias in vegetated areas from 11.2 m to 2.9 m (Table 3) and also reduces the RMSE by 46% to 7.6 m (Table 2). However, this improvement is not spatially consistent, with large errors still visible across the continents. The global correction method (Fig. 3(C)) is an incremental improvement over the static correction method and further reduces the ME and RMSE by over one metre to 1.2 m and 6.1 m respectively. This improvement is clearly visible over tropical forest regions such as the Amazon and Congo River Basins and in Indonesia and Papua New Guinea. Only small improvements over the global correction method are made by regionalizing the vegetation correction by climate zone or vegetation type (Figs. 4 and 5). While the overall RMSE improvements are only ~0.2 m for the climate correction and <0.1 m in the case of the vegetation correction method, larger improvements are experienced across the different continents. The climate correction outperforms all other methods in terms of ME with an overall ME of 0.3 m, while the global correction is next with 1.2 m. A visual comparison of the correction methods also highlights that the climate regionalized correction (Figs. 4(A) and 5(C)) outperforms the other methods. However, there are a few places where the vegetation-regionalized correction outperforms the climate correction, especially in The Andes and in China's Sichuan province.

From the analysis it is clear that the climate regionalized correction of vegetation of the SRTM DEM performs best, with the exception of a few small areas. However, the use of classification maps introduces artefacts along the classification boundaries and the increase in artefacts introduced by moving from five to fifteen f(VCF) models for the vegetation regionalized classification is not justifiable considering the small improvement that results- Fig. 5(C) and (D) are nearly identical. To reduce the impact of classification boundaries a simple averaging scheme can be used. The percentage of vegetation to be removed at any pixel is a weighted average based on the area covered by each classification in a 101 pixel (3 arc-second) square centred on the corresponding pixel. The size of square was determined by trial and error. While this scheme does not remove artefacts completely; it does significantly reduce their impact.

Other artefacts exist due to the spatial resolution of both the H_{VEG} and canopy density (VCF) products being much coarser than the 3 arc-seconds resolution of SRTM. Even after we downscale both the H_{VEG} and VCF maps to 3 arc-seconds, artefacts may exist around the edges of vegetation patches. However, to our knowledge, no finer resolution and coherent maps for global vegetation or canopy density exist. As our methodology ignores non-vegetated areas, artefacts may be introduced at the boundaries between vegetated and non-vegetated areas, where the elevation in the vegetated areas may now be slightly lower than that of the adjacent non-vegetated area.

Table 3
Vertical mean error (m) of RAW and corrected SRTM using different vegetation correction methods compared with ICESat GLA14 elevations in vegetated areas. Both averaged by VCF (1st number) and equal weight (2nd number) calculations are shown.

Region	Vegetation Correction Method				
	Raw	Static	Global	Climate	Vegetation
Europe	10.774/4.858	2.114/−1.445	0.744/−0.270	−0.653/−1.360	0.654/−0.391
Africa	10.838/4.299	2.491/−0.319	0.731/1.823	0.219/1.064	0.722/1.073
Asia	14.417/7.312	5.237/0.985	3.623/2.619	3.187/2.047	3.165/1.733
Southern Asia	15.857/7.376	5.783/0.913	3.801/2.185	2.417/1.287	3.051/1.631
Australia & New Zealand	14.325/4.335	5.438/−0.165	3.494/2.054	3.071/1.568	3.098/0.946
Pacific Islands	18.592/18.643	8.200/8.148	7.124/6.861	5.496/5.209	5.570/5.338
North America	8.459/3.749	1.293/−1.413	−0.089/−0.276	−1.482/−1.534	0.957/−0.290
South America	9.621/4.811	1.784/−0.797	0.308/0.749	−0.319/−0.038	0.247/0.209
Global	11.191/4.937	2.914/−0.398	1.178/1.251	0.294/0.402	1.215/0.694

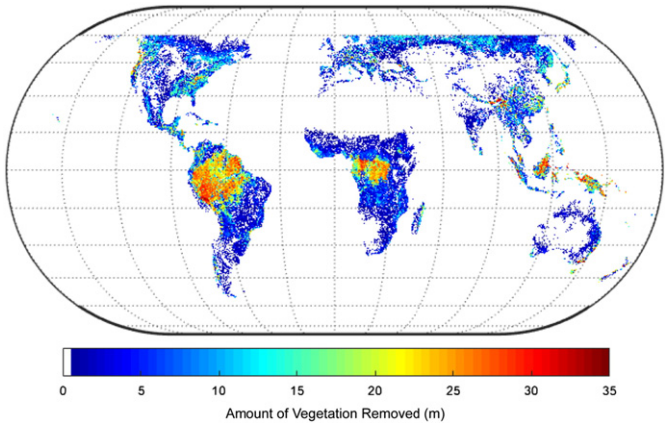

Fig. 6. Amount of vegetation removed (m) using the Power 1 vegetation removal function and climate regionalization.

We determine that the use of the Power 1 vegetation correction function with the climate zone classification produced the best result and from here on is referred to as 'Bare-Earth' SRTM. Fig. 6, shows the average amount of vegetation removed globally by using the Power 1 vegetation correction function with the climate zone classification. As expected from Figs. 3 and 4, the greatest amount of vegetation removal occurred in tropical forests, where it is known SRTM had the greatest vegetation bias. Fig. 7, shows the average amount of vegetation removed as a function of canopy density (VCF). As expected, the average amount of vegetation removed increases with increasing canopy density. This figure is truncated at a VCF percentage of 87 as there were insufficient data (<0.01%) after this value.

While the analysis to determine the best methodology has focused on continental and global scales, it is also useful to investigate how well the new 'Bare-Earth' SRTM performs over the main global vegetation types. Table 4 shows the root mean square errors of the original SRTM and the new 'Bare-Earth' SRTM compared with ICESat ground elevations over the 16 main vegetation types described by Broxton et al. (2014). With the exception of permanent wetlands, which account for only 1.29% of the world's landmass, the 'Bare-Earth' SRTM product outperforms the original SRTM dataset, with particularly large improvements in all Forest type vegetation, as would be expected.

Table 4
Comparison of the root mean square error (m) of the original and our 'Bare-Earth' SRTM by vegetation type.

Vegetation type	Original SRTM	'Bare-Earth' SRTM	Percentage of landmass
Evergreen needle leaf forest	11.714	6.454	1.94
Evergreen broadleaf forest	21.878	7.816	5.12
Deciduous needle leaf forest	12.440	7.350	1.40
Deciduous broadleaf forest	11.443	5.207	0.66
Mixed forests	16.686	7.353	4.74
Closed scrublands	10.150	6.250	0.06
Open scrublands	6.193	4.893	12.95
Woody savannahs	8.951	5.170	5.48
Savannahs	5.523	3.739	4.16
Grasslands	6.611	5.398	10.43
Permanent wetland	3.865	4.558	1.29
Croplands	4.414	3.839	6.09
Urban and built-up	5.595	3.980	0.32
Cropland/natural vegetation	7.435	4.566	4.07
Snow and ice	17.866	15.337	32.88
Barren or sparsely vegetated	8.611	7.041	8.42

3.3. Sample test cases

Fig. 8 shows the differences between the raw and 'Bare-Earth' SRTM DEMs for three five degree SRTM tiles along with cross-sectional profiles. While river channels are more defined in the SRTM DEM, floodplains are easier to distinguish in the new 'Bare-Earth' SRTM DEM. This effect is especially visible in the middle panel (Amazon basin).

The effect of removing the vegetation error is visible in the different plots for each of the three SRTM tiles. While the maximum amount of vegetation removed is similar across the three regions (36–44 m), the average vegetation removed is over 20 m in the Amazon (middle panel), approximately 14 m in the top panel and in the Congo (bottom panel).

The cross-sectional profiles show the vegetation contamination in the SRTM DEM compared with the new 'Bare-Earth' DEM. In the top panel, there are only small differences between the two DEMs; however, the differences are much larger for the cross-sectional profiles of the Amazon and Congo regions. In both regions, there are differences greater than 30 m. From the cross-sectional profiles, it is clear that the new 'Bare-Earth' SRTM DEM captures the floodplain extents more accurately and does not experience the same vegetation errors as the SRTM DEM. The use of this new product in hydrodynamic modelling will enable

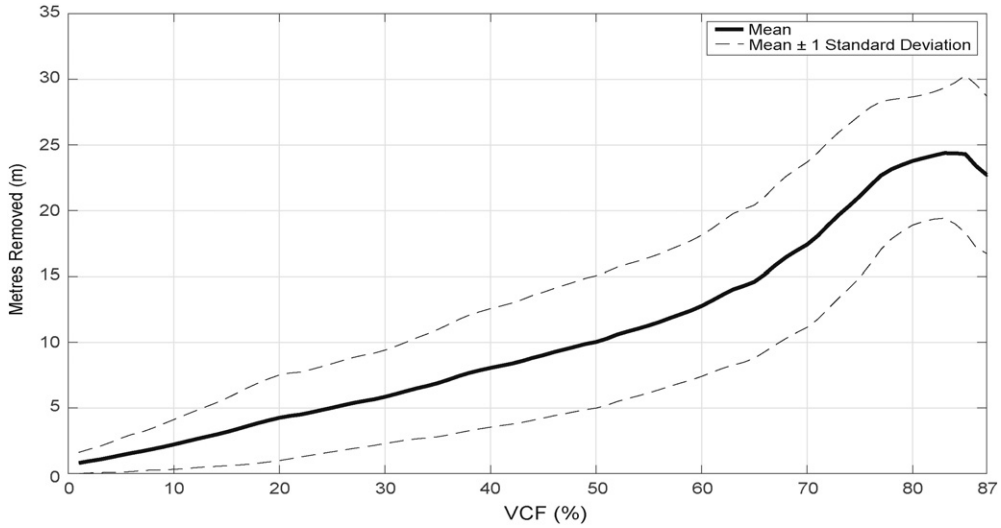

Fig. 7. Average metres removed (m) versus VCF (%) for the final 'Bare-Earth' SRTM DEM.

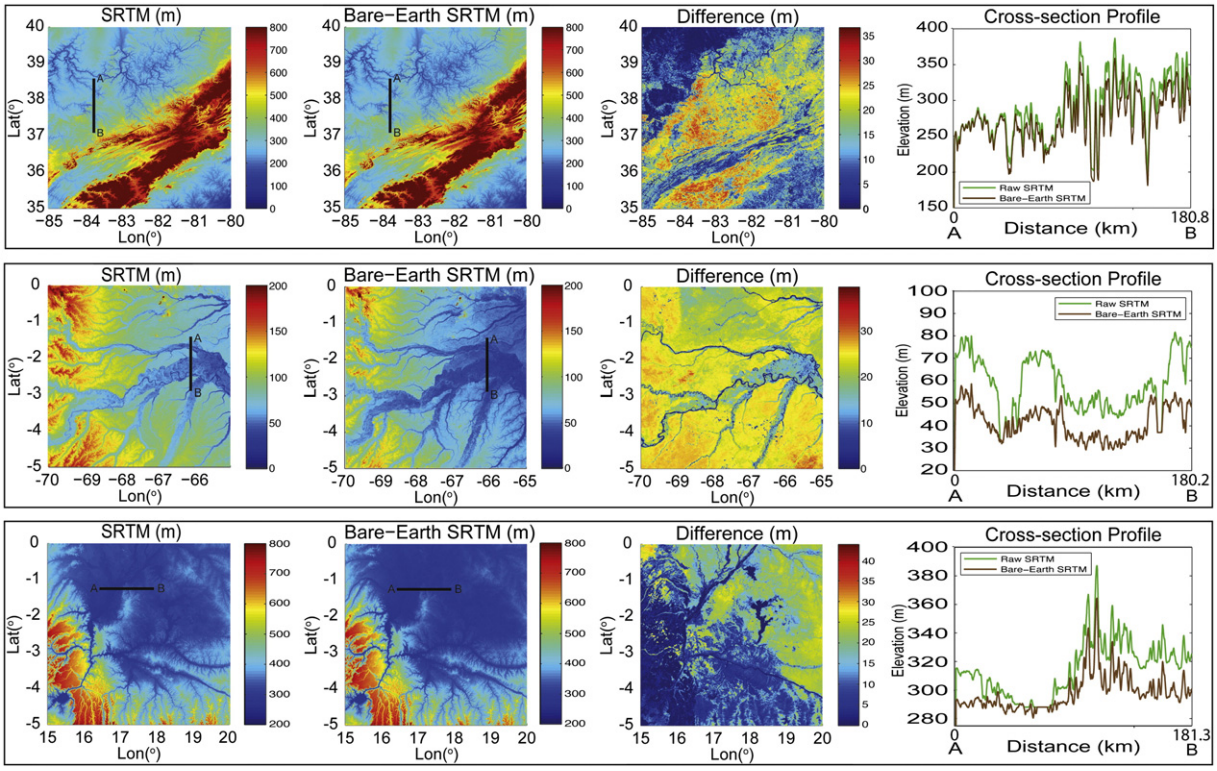

Fig. 8. Comparison of final 'Bare-Earth' SRTM DEM to the SRTM DEM for three 5° SRTM tiles, including difference between DEMs and smoothed cross-sectional profiles along A-B. Top Panel: SRTM grid 20_05 (North America). Middle Panel: SRTM grid 23_13 (Amazon Basin). Bottom Panel: SRTM grid 40_13 (Congo Basin).

the connectivity between the river channels and the floodplains to be more accurately modelled.

Fig. 9 shows a comparison of the 'Bare-Earth' SRTM DEM with the original SRTM for an area approximately 22 km by 32 km in Australia centred on −35.9 latitude and 145.2 longitude. Also shown are the corresponding VCF and H_{VEG} datasets. From this figure, it is clear that the method, proposed in this manuscript, reduces the elevations of the original SRTM in relation to the VCF and H_{VEG} datasets. However, the

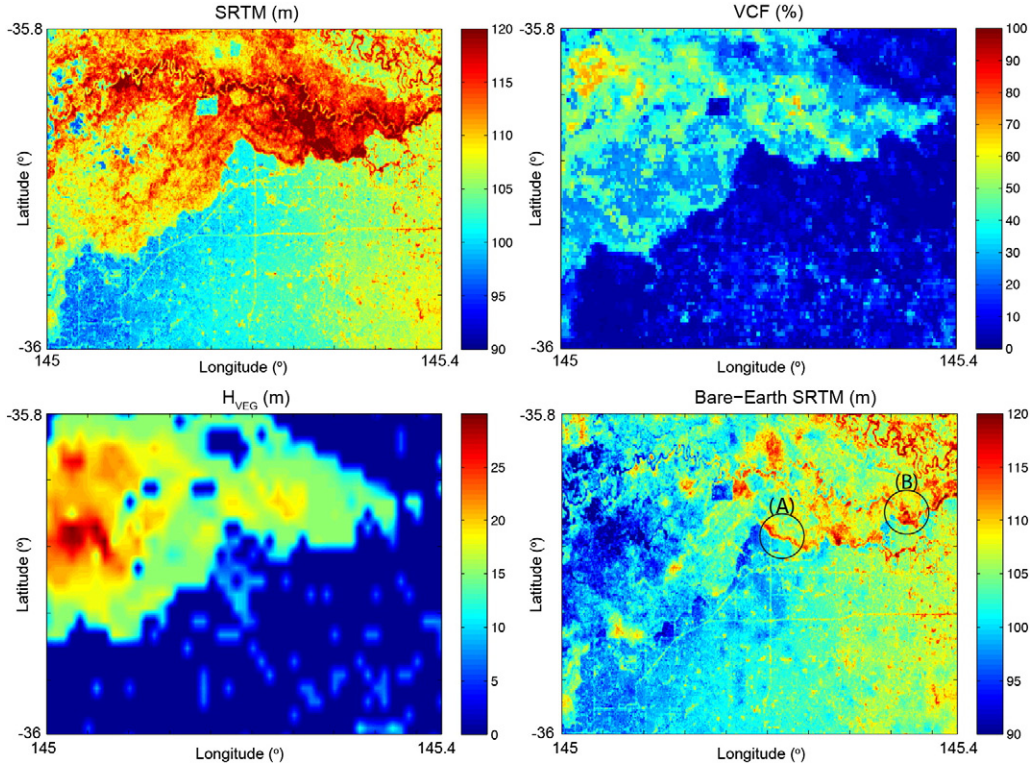

Fig. 9. Comparison of final 'Bare-Earth' SRTM DEM to the SRTM DEM for a region of Australia centred on latitude −35.9 and longitude 145.2. Also shown are the corresponding VCF and H_{VEG} datasets. Areas (A and B) showing limitations of the 'Bare-Earth' SRTM DEM are circled in bottom right tile.

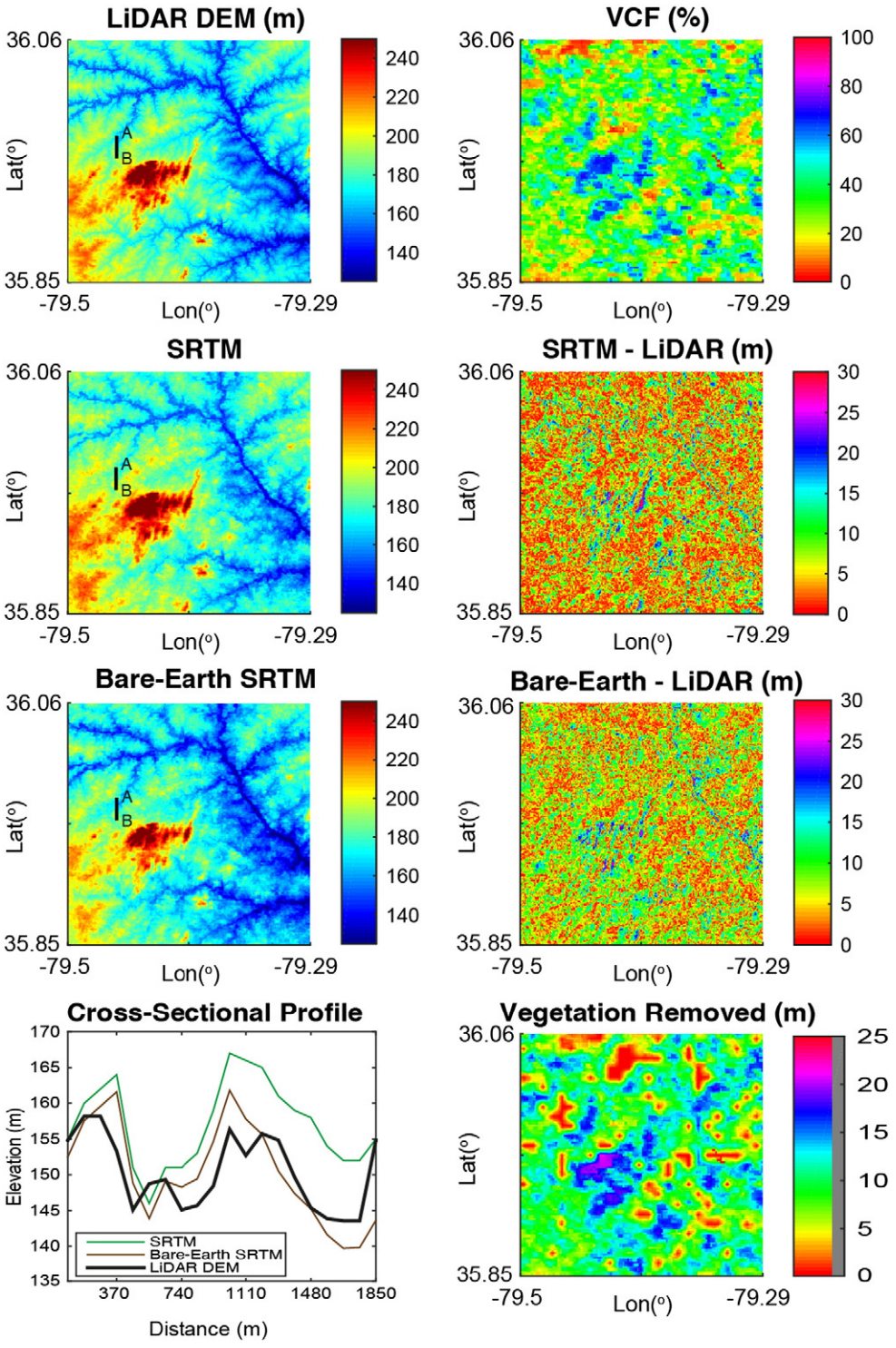

Fig. 10. Comparison of final 'Bare-Earth' SRTM DEM to both the SRTM DEMs and LiDIR DEM for a small region of Alamance County (North Carolina, USA), including a cross-sectional profiles along A-B for the three DEMs, differences between DEMs. The corresponding VCF data and the amount of vegetation removed from the original SRTM are also shown. LiDAR DEM obtained from the NC Flood Mapping Program (www.ncfloodmaps.com).

methodology and datasets used do have some limitations. Some of these limitations are highlighted in Fig. 8. Circle A highlights an area where our 'Bare-Earth' SRTM DEM produces some vegetation edge artefacts, while circle B highlights an area where the vegetation error has remained untreated. These artefacts are mainly due to the spatial resolution of the raw datasets used. While the 'Bare-Earth' SRTM DEM is not perfect, it is a marked improvement over the original SRTM DEM in vegetated area and we recommend that a suitable noise reduction filter is applied to the 'Bare-Earth' SRTM DEM before many applications to reduce the impact of these artefacts.

3.4. Validation with LiDAR based DEM

In Fig. 10, we compare the 'Bare-Earth' and SRTM DEMs to a LiDAR DEM, obtained from the North Carolina Flood Mapping Program (www.ncfloodmaps.com). The LiDAR DEM was aggregated from its

raw resolution of 20 ft (~6 m) to 3 arc-seconds and its vertical error is less than 10 cm at its raw resolution. Visually both SRTM based DEMs appear similar to the LiDAR DEM; however, from the cross-sectional profile it is clear that neither product is a perfect match to the LiDAR DEM. The SRTM DEM is generally higher than the LiDAR DEM and while the 'Bare-Earth' DEM tends to match the LiDAR DEM profile better, it also results in areas lower than the LiDAR DEM. However, as LiDAR DEMs are not globally available, our global 'Bare-Earth' SRTM DEM is needed for global studies whereas local studies will continue to benefit from their own detailed LiDAR studies.

4. Conclusion

This paper has presented a robust method to create the first 'Bare-Earth' global high resolution DEM based on SRTM data. Our 'Bare-Earth' DEM deals only with vegetation biases and does not remove biases due to built structures. It should be noted that SRTM is a digital surface model and that for many applications surface feature/artefacts caused by vegetation canopies, which are present in all previous SRTM releases to date, cause significant errors. While there have been studies that have corrected this error for small regions, to our knowledge, no one has attempted this globally. For example, a 1 arc-second vegetation corrected SRTM product is available for Australia (http://www.ga.gov.au/metadata-gateway/metadata/record/69816/) but not over a wider area.

To correct for vegetation errors in the SRTM DEM, we utilized multiple remote sensing datasets. For a spatial representation of ground elevations we used the ICESat GLA14 land product. We used the Simard et al. (2011) vegetation height map for an estimate of canopy heights and the Hansen et al. (2003) Vegetation Continuous Field (VCF) as a proxy for canopy density.

We tested five different vegetation correction functions ranging from a simple linear model to power law and exponential functions and find that only the Power 1 model (Eq. (6)) did not introduce artefacts at low VCF values. We then applied the Power 1 vegetation correction function both globally and regionally, with regions defined either by climate or vegetation type. We compared each of these three methods with a static correction (Baugh et al., 2013).

We conclude that subtracting any vegetation height from the original SRTM DEM reduces the vegetation errors. The static correction reduced the global mean error and root mean square errors by 8.3 m and 6.5 m respectively. However, this method was spatially inconsistent, whilst all three methods developed in this paper (global and two regional classification methods) were spatially consistent and reduced significantly the errors in the SRTM DEM with improvements in mean error and root mean square error of 10.9 m and 8.2 respectively over the SRTM when averaged by VCF values. We determined that the use of a climate classification and the Power 1 vegetation correction function results in the best method for correcting the vegetation errors. Using a correction method regionalized according to climate type and the Power 1 vegetation correction function resulted in reductions of approximately 58% and 98% in RMSE and ME respectively.

The final 'Bare-Earth' SRTM DEM has global RMSE and global ME equal to 5.9 m and 0.29 m respectively in vegetated areas when compared with ICESat elevations. When compared by vegetation type, the final 'Bare-Earth' DEM outperforms the original SRTM over 98.7% of the vegetated landmass. While this manuscript utilizes the SRTM DEM dataset, the methodology used is valid for other near global DEMs.

The 'Bare-Earth' SRTM DEM has been computed globally at 3 arc-seconds resolution and is available for non-commercial use. The freely released product is un-filtered; therefore, for some applications a noise reduction filter might need to be applied to the DEM. Once the 1 arc-second SRTM DEM is available we intend to release a 1 arc-second 'Bare-Earth' SRTM DEM.

Acknowledgments

The first author was supported by the Leverhulme Trust grant RPG-409. The second and third authors were supported by NASA SWOT Science Definition Team grant NNX13AD96G. Douglas Alsdorf is supported by the Ohio State University. Paul Bates was supported by UK Natural Environment Research Council grant NE/M007766/1 to the "Open access global flood hazard layers" project.

The 'Bare-Earth' SRTM v1 DEM is available freely from http://data.bris.ac.uk/data/dataset/10tv0p32gizt01nh9edcjzd6wa.

References

Baldocchi, D., Falge, E., Gu, L., Oison, R., Hollinger, D., Running, S., Anthoni, P., Bernhofer, C., Davis, K., Evans, R., et al. (2001). FLUXNET: A new tool to study the temporal and spatial variability of ecosystem-scale carbon dioxide, water vapor, and energy flux densities. *Bulletin of the American Meteorological Society*, *82*(11), 2415–2434. http://dx.doi.org/10.1175/1520-0477(2001)082<2415:FANTTS>2.3.CO;2.

Bamber, J. L. (1994). A Digital Elevation Model of the Antarctic ice sheet derived from ERS•l altimeter data and comparison with terrestrial measurements. *Annals of Glaciology*, *20*(1), 48–54. http://dx.doi.org/10.3189/172756494794586934.

Baugh, C. A., Bates, P. D., Schumann, G., & Trigg, M. A. (2013). SRTM vegetation removal and hydrodynamic modeling accuracy. *Water Resources Research*, *49*(9), 5276–5289. http://dx.doi.org/10.1002/wrcr.20412.

Berry, P. A. M., Garlick, J. D., & Smith, R. G. (2007). Near-global validation of the SRTM DEM using satellite radar altimetry. *Remote Sensing of Environment*, *106*(1), 17–27. http://dx.doi.org/10.1016/j.rse.2006.07.011.

Bhang, K. J., Schwartz, F. W., & Braun, A. (2007). Verification of the vertical error in C-band SRTM DEM using ICESat and Landsat-7, Otter Tail County, MN. *IEEE Transactions on Geoscience and Remote Sensing*, *45*(1), 36–44. http://dx.doi.org/10.1109/TGRS.2006.885401.

Broxton, P. D., Zeng, X., Sulla-Menashe, D., & Troch, P. A. (2014). A global land cover climatology using MODIS data. *Journal of Applied Meteorology and Climatology*, *53*(6), 1593–1605. http://dx.doi.org/10.1175/JAMC-D-13-0270.1.

Carabajal, C. C., & Harding, D. J. (2005). ICESat validation of SRTM C-band Digital Elevation Models. *Geophysical Research Letters*, *32*(22), L22S01. http://dx.doi.org/10.1029/2005GL023957.

De Ruyver, R. (2004). *DEM optimization for hydrological modelling using SRTM for the "Pantanal" region, Brazil.* Enschede, Netherlands: International Institute for Geo-infromation Science and Earth Observation.

DiMiceli, C. M., Carroll, M. L., Sohlberg, R. A., Huang, C., Hansen, M. C., & Townshend, J. R. G. (2011). *Annual Global Automated MODIS Vegetation Continuous Fields (MOD44B) at 250 m spatial resolution for data years beginning day 65, 2000–2010, collection 5 percent tree cover.* Univ. Md. Coll. Park.

Farr, T. G., & Kobrick, M. (2000). Shuttle Radar Topography Mission produces a wealth of data. *EOS. Transactions of the American Geophysical Union*, *81*(48), 583–585. http://dx.doi.org/10.1029/EO081i048p00583.

Farr, T. G., Rosen, P. A., Caro, E., Crippen, R., Duren, R., Hensley, S., Kobrick, M., Paller, M., Rodriguez, E., Roth, L., et al. (2007). The Shuttle Radar Topography Mission. *Reviews of Geophysics*, *45*(2), RG2004. http://dx.doi.org/10.1029/2005RG000183.

Gallant, J., Read, A., & Dowling, T. (2012). Removal of tree offsets from SRTM and other digital surface models. *The International Archives of the Photogrammetry, Remote Sensing and Spatial Information Sciences*, *1*, 275–280.

Hall, A. C., Schumann, G. J. -P., Bamber, J. L., Bates, P. D., & Trigg, M. A. (2012). Geodetic corrections to Amazon River water level gauges using ICESat altimetry. *Water Resources Research*, *48*(6).

Hansen, M. C., DeFries, R. S., Townshend, J. R. G., Carroll, M., Dimiceli, C., & Sohlberg, R. A. (2003). Global percent tree cover at a spatial resolution of 500 meters: First results of the MODIS Vegetation Continuous Fields Algorithm. *Earth Interactions*, *7*(10), 1–15. http://dx.doi.org/10.1175/1087-3562(2003)007<0001:GPTCAA>2.0.CO;2.

Harding, D. J., & Carabajal, C. C. (2005). ICESat waveform measurements of within-footprinttopographic relief and vegetation vertical structure. *Geophysical Research Letters*, *32*(21).

Hirabayashi, Y., Mahendran, R., Koirala, S., Konoshima, L., Yamazaki, D., Watanabe, S., ... Kanae, S. (2013). Global flood risk under climate change. *Nature Climate Change*, *3*(9), 816–821. http://dx.doi.org/10.1038/nclimate1911.

Jarihani, A. A., Callow, J. N., McVicar, T. R., Van Niel, T. G., & Larsen, J. R. (2015). Satellite-derived Digital Elevation Model (DEM) selection, preparation and correction for hydrodynamic modelling in large, low-gradient and data-sparse catchments. *Journal of Hydrology*, *524*, 489–506. http://dx.doi.org/10.1016/j.jhydrol.2015.02.049.

Jarvis, A., Reuter, H. I., Nelson, A., & Guevara, E. (2008). Hole-filled SRTM for the globe version 4. Available CGIAR-CSI SRTM 90m Database http://srtm.csi.cgiar.org

Kenyi, L. W., Dubayah, R., Hofton, M., & Schardt, M. (2009). Comparative analysis of SRTM–NED vegetation canopy height to LiDAR-derived vegetation canopy metrics. *International Journal of Remote Sensing*, *30*(11), 2797–2811. http://dx.doi.org/10.1080/01431160802555853.

Krabill, W. B., Collins, J. G., Link, L. E., Swift, R. N., & Butler, M. L. (1984). Airborne laser topographic mapping results. *Photogrammetric Engineering and Remote Sensing*, *685–694*.

Lefsky, M. A. (2010). A global forest canopy height map from the moderate resolution imaging spectroradiometer and the geoscience laser altimeter system. *Geophysical Research Letters*, *37*(15), L15401. http://dx.doi.org/10.1029/2010GL043622.

Milly, P. C. D., Wetherald, R. T., Dunne, K. A., & Delworth, T. L. (2002). Increasing risk of great floods in a changing climate. *Nature*, *415*(6871), 514–517. http://dx.doi.org/10.1038/415514a.

Moore, I. D., Grayson, R. B., & Ladson, A. R. (1991). Digital terrain modelling: A review of hydrological, geomorphological, and biological applications. *Hydrological Processes*, *5*(1), 3–30. http://dx.doi.org/10.1002/hyp.3360050103.

O'Loughlin, F. E., Neal, J., Yamazaki, D., & Bates, P. D. (2016). ICESat-derived inland water surface spot heights. *Water Resources Research*, *52*. http://dx.doi.org/10.1002/2015WR018237.

O'Loughlin, F., Trigg, M. A., Schumann, G. -P., & Bates, P. D. (2013). Hydraulic characterization of the middle reach of the Congo River. *Water Resources Research*, *49*(8), 5059–5070.

Paiva, R. C. D., Buarque, D. C., Collischonn, W., Bonnet, M. -P., Frappart, F., Calmant, S., & Bulhões Mendes, C. A. (2013). Large-scale hydrologic and hydrodynamic modeling of the Amazon River basin. *Water Resources Research*, *49*(3), 1226–1243. http://dx.doi.org/10.1002/wrcr.20067.

Paiva, R. C. D., Collischonn, W., & Tucci, C. E. M. (2011). Large scale hydrologic and hydrodynamic modeling using limited data and a GIS based approach. *Journal of Hydrology*, *406*(3–4), 170–181. http://dx.doi.org/10.1016/j.jhydrol.2011.06.007.

Peel, M. C., Finlayson, B. L., & McMahon, T. A. (2007). Updated world map of the Köppen-Geiger climate classification. *Hydrology and Earth System Sciences*, *11*(5), 1633–1644. http://dx.doi.org/10.5194/hess-11-1633-2007.

Pinel, S., Bonnet, M. P., Santos Da Silva, J., Moreira, D., Calmant, S., Satgé, F., & Seyler, F. (2015). Correction of interferometric and vegetation biases in the SRTMGL1 spaceborne DEM with hydrological conditioning towards improved hydrodynamics modeling in the Amazon Basin. *Remote Sensing*, *7*(12), 16108–16130.

Rabus, B., Eineder, M., Roth, A., & Bamler, R. (2003). The Shuttle Radar Topography Mission—A new class of Digital Elevation Models acquired by spaceborne radar. *ISPRS Journal of Photogrammetry and Remote Sensing*, *57*(4), 241–262. http://dx.doi.org/10.1016/S0924-2716(02)00124-7.

Rodríguez, E., Morris, C. S., & Belz, J. E. (2006). A global assessment of the SRTM performance. *Photogrammetric Engineering and Remote Sensing*, *72*(3), 249–260. http://dx.doi.org/10.14358/PERS.72.3.249.

Sanders, B. F. (2007). Evaluation of on-line DEMs for flood inundation modeling. *Advances in Water Resources*, *30*(8), 1831–1843. http://dx.doi.org/10.1016/j.advwatres.2007.02.005.

Schumann, G. J. -P., Bates, P. D., Neal, J. C., & Andreadis, K. M. (2014). Technology: Fight floods on a global scale. *Nature*, *507*(7491), 169. http://dx.doi.org/10.1038/507169e.

Schutz, B. E., Zwally, H. J., Shuman, C. A., Hancock, D., & DiMarzio, J. P. (2005). Overview of the ICESat mission. *Geophysical Research Letters*, *32*(21).

Sexton, J. O., Song, X. -P., Feng, M., Noojipady, P., Anand, A., Huang, C., Kim, D. -H., Collins, K. M., Channan, S., DiMiceli, C., et al. (2013). Global, 30-m resolution continuous fields of tree cover: Landsat-based rescaling of MODIS Vegetation Continuous Fields with LiDAR-based estimates of error. *International Journal of Digital Earth*, *6*(5), 427–448. http://dx.doi.org/10.1080/17538947.2013.786146.

Shimada, M., Itoh, T., Motooka, T., Watanabe, M., Shiraishi, T., Thapa, R., & Lucas, R. (2014). New global forest/non-forest maps from ALOS PALSAR data (2007–2010). *Remote Sensing of Environment*, *155*, 13–31. http://dx.doi.org/10.1016/j.rse.2014.04.014.

Simard, M., Pinto, N., Fisher, J. B., & Baccini, A. (2011). Mapping forest canopy height globally with spaceborne LiDAR. *Journal of Geophysical Research – Biogeosciences*, *116*(G4), G04021. http://dx.doi.org/10.1029/2011JG001708.

Wilson, M., Bates, P., Alsdorf, D., Forsberg, B., Horritt, M., Melack, J., ... Famiglietti, J. (2007). Modeling large-scale inundation of Amazonian seasonally flooded wetlands. *Geophysical Research Letters*, *34*(15).

Zwally, H. J., Schutz, B., Abdalati, W., Abshire, J., Bentley, C., Brenner, A., Bufton, J., Dezio, J., Hancock, D., Harding, D., et al. (2002). ICESat's laser measurements of polar ice, atmosphere, ocean, and land. *Journal of Geodynamics*, *34*(3–4), 405–445. http://dx.doi.org/10.1016/S0264-3707(02)00042-X.